Using self-assembled monolayer technology to probe the mechanical response of the fiber interphase-matrix interphase interface

G. A. HOLMES [1,*], E. FERESENBET [2] and D. RAGHAVAN [2]

[1] *National Institute of Standards and Technology, 100 Bureau Drive M/S 8543, Gaithersburg, MD 20899-8543, USA*
[2] *Howard University, Chemistry Department, Washington, DC 20059, USA*

Abstract—In this paper, a brief review of the fiber–matrix interphase/interface region is given for carbon- and glass-fiber composites. The substructure of the interphase/interface region is discussed in terms of three interphases: (a) the fiber interphase (FI), (b) the sizing interphase (SI), and (c) the matrix interphase (MI), and two interface regions: (a) the FI-SI interface and (b) the SI-MI interface. These substructures are a synthesis of the ideas advanced by Ishida and Koenig and Drzal. The schematic model of interphase deformation behavior originally given by Bascom is reconstructed to include research results from the above researchers. To systematically probe adhesion at the SI-MI interface, functionalized self-assembled monolayers (SAMs) using bonding and non-bonding C_{11}-type trichlorosilanes are prepared using the research of Menzel and Heise, and that of Cave and Kinloch as a guide. Results from this research are compared with short chain bonding and non-bonding silanes prepared by aqueous and non-aqueous deposition processes. The data were interpreted using the mechanisms proposed by Sharpe, Ishida and Koenig, and Drzal and the mathematical equation proposed by Nardin and Ward. For the non-bonding short-chain silane deposited by aqueous deposition, 90% of the adhesion was found to be due to mechanical interlocking, with the remaining adhesion due to physicochemical interactions. For the bonding short-chain silane deposited by aqueous deposition, the interface strength relative to the non-bonding short-chain silane increased by 31%. However the interfacial shear strength (IFSS) of this system was approximately 40% lower than the comparable bonding SAM interface. This difference was interpreted in terms of the propensity of the C_3-alkylamine to form cyclic ring structures in the MI region as described by Ishida, Koenig, *et al*. The SAM data also indicates that 70–85% of the maximum IFSS is obtained with 25–50% of the surface covered with functional groups. This suggests that steric hindrance, due to the size of the DGEBA molecules, restricts access to the functional groups on the surface. Therefore, only 35% of the surface functional groups are accessible for bonding in the DGEBA/m-PDA epoxy resin system.

Keywords: Self-assembled monolayer; adhesion; interface strength; silane coupling agent; interphase; interface; matrix; glass fiber; carbon fiber.

---

*To whom correspondence should be addressed. E-mail: gale.holmes@nist.gov

1. INTRODUCTION

With the potential widespread use of composites in structural applications, several conferences and symposia [1–5], journals [6, 7], and books [8–10] have been devoted to research of the fiber–matrix interface/interphase region. This region controls the stress-transfer between the fiber and matrix as well as the initial failure modes in composite structures by effecting the 'cross-coupling' between the fiber and matrix. Although Sharpe [11] was the first to note the existence of an interphase region in an adhesive joint, much of our understanding about the morphology of the interphase region and its affect on the mechanical response and failure of composites is due to the research of Ishida and Koenig [12–16], Plueddemann [17, 18], and Drzal *et al.* [19–23]. Boerio [24–26], who investigated extensively the morphology and stability of silanes absorbed onto metallic substrates, has also made important contributions to our understanding of the interface/interphase region.

Sharpe and Drzal have ascribed adhesion in the interphase region to (a) mechanical interlocking, (b) physicochemical interactions, (c) chemical bonding, and (d) mechanical deformation of the fiber–matrix interphase region. In 1987, Nardin and Ward [27] suggested that the contributions of the first three parameters to fiber–matrix interphase adhesion between polyethylene fiber and low viscosity epoxy resin was additive.

$$\tau_i = \tau_M + \tau_{PCI} + \tau_{CB}, \tag{1}$$

where τ_i denotes the total fiber–matrix adhesion as measured by the interphase strength parameter; τ_M denotes the adhesion at the fiber–matrix interphase due to mechanical interlocking; τ_{PCI} denotes the adhesion at the fiber–matrix interphase due to physicochemical interactions; and τ_{CB} denotes the adhesion at the fiber–matrix interphase due to chemical bonding.

Nardin and Ward proposed that the contribution to interfacial adhesion due to physicochemical interactions could be quantified by the following expression:

$$\tau_{PCI} = \alpha(\gamma_S - \gamma_C), \tag{2}$$

where γ_S denotes the surface free energy of the treated fiber; γ_C denotes the critical surface tension of the fiber; α is a numerical constant obtained from plotting τ_{PCI} versus γ_S.

In addition, Nardin and Ward proposed that the contribution to interfacial adhesion due to mechanical interlocking is related to the rugosity of the fiber surface and the maximum contribution to interfacial adhesion from physicochemical interactions ($\tau_{PCI}^{\max}$).

$$\tau_M = ae + \tau_{PCI}^{\max}, \tag{3}$$

where e denotes the mean depth in μm of the pits or valleys on the fiber surface; and a is a constant (MPa/μm).

These authors noted that it is difficult to separate the contributions to interfacial adhesion by the second and third terms in equation (1). In addition, they speculated

that the contribution to interfacial adhesion by chemical bonding is related to the number of chemical bonds in the fiber–matrix interphase region. Several researchers have discussed the role of chemical bonding in fiber–matrix adhesion and, at present, its role appears to depend on the specifics of the composite system.

There have been few fundamental studies quantifying the contribution of each of the above parameters to fiber–matrix interface adhesion. The major obstacles have been the complexity of the interphase region, the lack of research tools that control the competing contributions to interphase adhesion, and the inability to quantify the size and physical properties of the fiber–matrix interphase region. Using recently developed functionalized self-assembled monolayer (SAM) technology [28–30], a molecular tool capable of reducing the complexity and controlling the morphology of the interphase region, we will focus, in this research paper, on the first two obstacles as they relate to glass fiber composites (GFCs).

1.1. Background information on the fiber–matrix interphase/interface region

Since the inception of the interphase concept by Sharpe in 1972, considerable research has been devoted to understanding the morphology and function of the fiber–matrix interphase region in composites. As an example, Manson and Sperling [31] reviewed interphase research prior to 1976 and discussed in length the role of the matrix, interphase properties, and interphase adhesion on composite toughness. In 1978, Ishida and Koenig [12] reported the components of the interphase region in GFCs as (a) the glass/coupling agent interface, (b) the coupling agent, and (c) the coupling agent/matrix. Subsequent research by Drzal [19–22] on carbon fiber composites (CFCs) extended the three-dimensional description of the interphase region to include a fiber interphase (FI) and a matrix interphase (MI). Noting that the 'sizing' used on carbon fibers is different from the 'sizing' used on glass fibers, we adopt the following nomenclature that includes the features of both interphase models: (a) the fiber interphase (FI), (b) the fiber interphase (FI)-sizing interphase (SI) interface, (c) the sizing interphase (SI), (d) the sizing interphase (SI)-matrix interphase (MI) interface, and (e) the matrix interphase (MI). Therefore, the fiber matrix interphase region potentially consists of three 3D interphases (FI, SI, and MI) and two 2D regions of contact (FI-SI interface and SI-MI interface).

In general, the FI includes any surface features on the reinforcing fibers (morphological and chemical) that differ from the bulk fiber properties [22]. These surface features are often manipulated to enhance adhesion between the fiber and matrix and to enhance environmental stability of the interphase region.

The composition and morphology of the SI depends on the fiber type. In GFCs, the cross-coupling technology between the fiber and matrix is generally accomplished by the use of silane coupling agents and film forming technology [12]. In CFCs, surface modification of the fiber followed by the application of a 100–200 nm resin coating usually effects the cross-coupling between the fiber and the matrix [20].

The MI includes the region near the FI-MI interface whose network properties differ appreciably from the bulk matrix properties. This region as defined by Drzal includes matrix that may have chemical and morphological features different from the bulk matrix, impurities, unreacted polymer components, and non-polymerized matrix additives, etc. The MI region is believed by Bascom [32] to be less than 1 μm in thickness and have a gradient of properties that extend from the SI-MI interface to the bulk resin.

In the interphase region, voids, adsorbed gases, and surface chemical groups can exist in addition to chemical and physical interactions between the fiber and matrix [22]. The MI will generally follow the topology of the embedded fiber or the applied sizing, with this topology providing sites for adhesion through mechanical keying by the resin and chemical and physicochemical interactions between the resin and the fiber surface or the sizing. Hence, the SI-MI interface or the FI-MI interfaces controls the rate of stress transfer between the matrix and fiber.

As previously noted, the specific influence of the various contributors to adhesion at the fiber–matrix interphase appears to depend on the type of composite system. In discussing what is currently known about carbon- and glass-fiber interphases, the authors will briefly review each composite type separately.

1.2. Carbon fiber composites

1.2.1. The fiber interphase (FI) region. For carbon fibers, adhesion is typically enhanced by electrochemical oxidation or other proprietary treatments of the carbon fiber surface and possibly by the inclusion of functionalized organic molecules (e.g. a 100–200 nm layer of epoxy resin) [19–22]. Drzal has demonstrated the need for treating carbon fiber surfaces by showing that the surface of a type-AU carbon fiber has a mechanically weak outer layer that limits the maximum interfacial shear strength (IFSS) that is obtained with this fiber. This carbon fiber, also known as a type-II carbon fiber, is graphitized at 1500°C. In his research, Drzal added the 'U' designation to denote the fiber before it was treated to enhance fiber-matrix interphase/interface adhesion. Fiber fracture in model composites composed of AU carbon fibers (with and without sizing) was accompanied by the propagation of interfacial cracks along the fragment length in the weak FI region. Therefore, the weak outer layer of the type-AU carbon fiber (FI region) precludes failure in the other interphase regions or interfaces that may exist in the substructure of the fiber–matrix interphase region and limits the obtainable fiber–matrix interfacial shear strength.

Although carbon fiber surface treatments remove this weak outer layer, this procedure adds surface chemical groups (e.g. ketones, acid groups, hydroxyl groups, amine groups) that increase adhesion with the resin. Since these functional groups are only on the surface, there exists a small FI region at the carbon fiber surface that is well bonded to the bulk carbon fiber. These carbon fibers are denoted type-AS by Drzal, where the 'S' denotes surface treatment. From his studies, Drzal concluded that the increased adhesion resulting from surface treatments of carbon

fibers is primarily due to the removal of the weak outer layer of graphitic carbon. Covalent bonding, which was estimated by Drzal to involve less than 5% of the available sites on the carbon fiber surface, increased adhesion by 14% relative to the type-AU carbon fiber adhesion. Interfacial failure was also observed in AS carbon fiber model composites. Drzal's research indicates that interfacial failure occurs at the FI-MI interface, since the FI region is well bonded to the bulk carbon fiber.

1.2.2. The matrix interphase (MI) and sizing interphase (SI) regions. In carbon fibers the simplest MI region is formed by the direct interaction of the matrix, typically an epoxy-amine resin, with the surface-treated carbon fiber. Hence, the fiber and matrix interact to form an interphase that is not influenced by an epoxy compatible sizing (i.e. no SI). As noted above, FI-MI interface failure was observed, even though interfacial shear strength increased by a fraction of 60% relative to the untreated fibers.

For this system, Palmese and McCullough [33] used thermodynamic and kinetic arguments to analyze the role of preferential adsorption and diffusion in the formation of the interphase region in thermosetting composites. These authors concluded that a thermodynamic driving force for the preferential adsorption of amines onto carbon fiber surfaces for epoxy-amine mixtures exists. However, their kinetic analyses indicate that preferential surface adsorption of amine is not sufficient to explain the existence of a MI region larger than one monolayer. Hence, a more sophisticated thermodynamic treatment maybe needed to describe MI region formation.

The coating of a surface-treated carbon fiber, designated AS-1 and AS-4 by Drzal, with a 100–200 nm thick layer of diglycidyl ether of bisphenol-A (DGEBA) resin, designation AS-1C and AS-4C, introduces a SI interphase that has the potential to diffuse into the bulk matrix during curing. Depending on the extent of the diffusion process, the distinction between the SI and MI would be blurred and a clear SI-MI interface would be nonexistent. Drzal found that this procedure increased fiber–matrix adhesion, by an additional fraction of at least 20% relative to the model composites composed of uncoated fibers (AS-1 and AS-4), at the expense of changing the failure mode during fiber fracture from interfacial to matrix crack formation [19, 20, 22].

By adding the resin layer, the amine-epoxy stoichiometry in the MI region may be altered from stoichiometric proportions. This is believed to occur by the inter-diffusion of the 100–200 nm DGEBA resin layer and the surrounding stoichiometric epoxy resin. Investigating the effect of epoxide-amine stoichiometry on matrix stiffness and fracture toughness, Drzal suggests that the inter-diffusion of the 100–200 nm DGEBA resin layer and the stoichiometric epoxy resin creates an epoxide rich MI/SI region with higher modulus and lower fracture toughness (see Fig. 1). The dependence of the fiber–matrix interphase strength on matrix stiffness has been shown theoretically in Cox-type shear-lag models and Drzal has
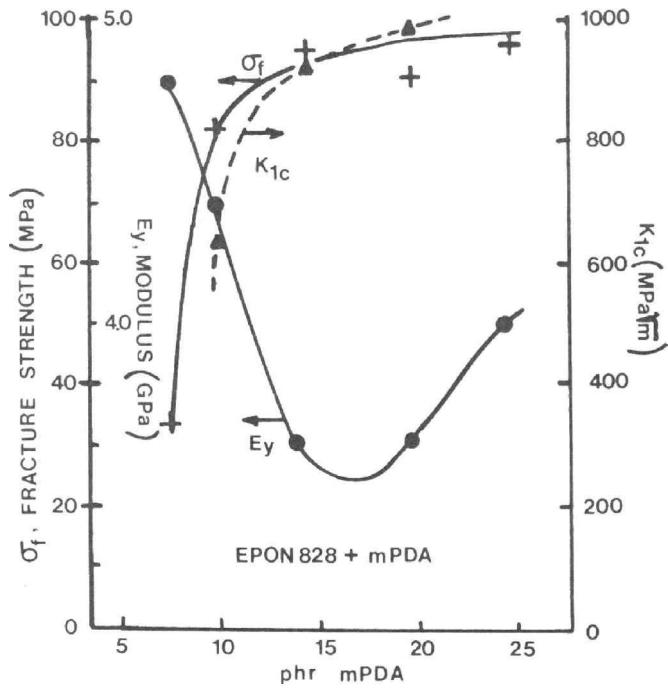
Figure 1. Initial tensile modulus (E_y), fracture strength (σ_f) and fracture toughness (K_{1C}) of Epon 828/mPDA mixtures as a function of parts per hundred resin (phr) of m-PDA. [20] (reprinted with permission).

found reasonable agreement with the dependencies predicted by these models and experimental data.

Palmese and McCullough [33] also treated this system theoretically. These researchers suggest that the characteristic time for diffusion of the resin coating is much slower than the characteristic epoxide-amine reaction time. Hence, a sharp SI-MI interface will exist between the SI and MI interphases rather than the SI/MI gradient interphase speculated by Drzal. This suggests that the DGEBA coating (SI region) has the properties of an uncatalyzed homopolymerized DGEBA resin (i.e. the interphase will be more brittle than that predicted by Drzal's diffusion model).

1.2.3. The fiber interphase-matrix interphase (FI-MI) interface. A systematic investigation into adhesion at the FI-MI interface has been performed by Drzal *et al.* [19]. Drzal observed that adhesion in untreated and treated carbon fibers is greatly influenced by the initial graphitization process. In his investigation, type-A (again, type-II — graphitized at 1500°C) and type-HM (also known as type-I — graphitized at 2600°C) carbon fibers were used. He observed that the main structural elements of carbon fibers, graphitic ribbons, are oriented approximately parallel to the fiber axis with graphitic crystallite size in the graphitic ribbons increasing with graphitization temperature. When compared to the type-HM carbon fibers, the
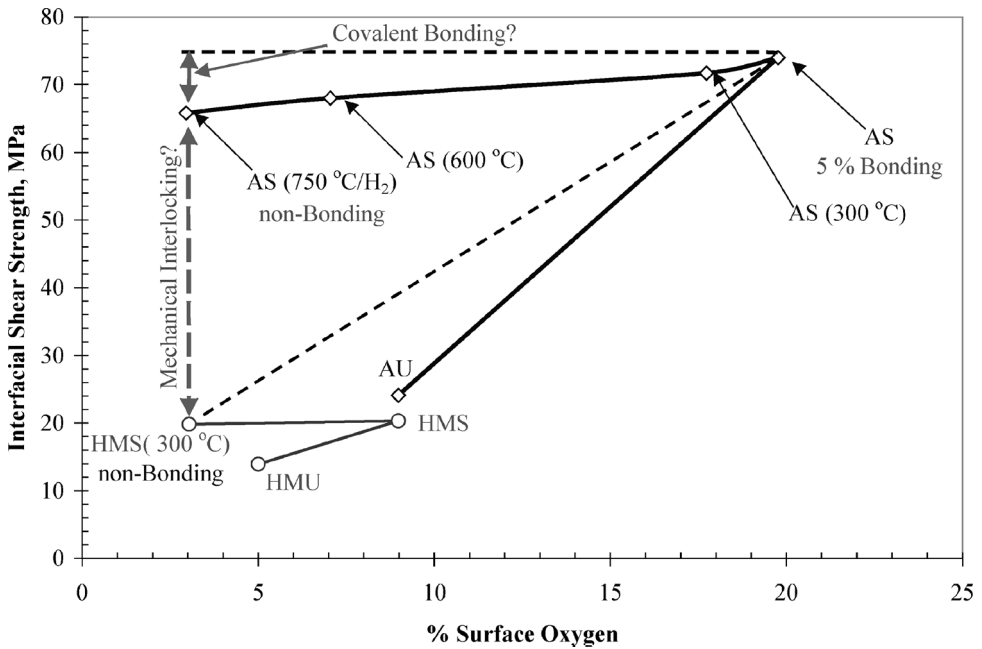
Figure 2. Interfacial shear strength plotted as a function of surface oxygen concentration determined by ESCA for type A and HM fibers (adapted from Ref. [19]).

shorter graphitic layers in the type-A fibers have the net effect of producing more corners and crystallite edges on the fiber surface. In addition, a weak outer layer (discussed above) is produced that, if not removed by treatment, limits the IFSS of a composite by causing FI failure.

The higher number of corners and crystallite edges in the type-A fibers provides additional sites for the formation of functional groups (e.g. carboxylic acid, phenolic type, hydroxylic, lactones, amines, and carbonylic) [34–36]. As a result, the IFSS in composites composed of untreated A-type fibers (AU) is higher than a similar composite with untreated HM-type fibers (HMU) (see Fig. 2). In this figure, fiber designations with parentheses and a temperature inside denotes the vacuum heat treatment temperature used by Drzal to remove oxygen groups from the fiber surface (e.g. AS (600°C)). The '/H_2' denotes that this heat treatment was performed in a reducing atmosphere of hydrogen. The dash line, drawn by the NIST author, between the AS and HMS (300°C) carbon fibers provides a visual connection to show the reader the two surface treated fibers that have the highest and lowest IFSS. The parallel dash line facilitates the visual assessment of the amount of IFSS due to covalent bonding.

It is known that epoxy resins can react with carboxylic acids, phenols, hydroxyl groups, acid anhydrides and amines [37, 38]. Research also indicates that carboxylic acids are the most abundant functional group on the carbon fiber surface, followed by phenols [35, 36, 39]. Hence, it is generally accepted that the chemical bonding
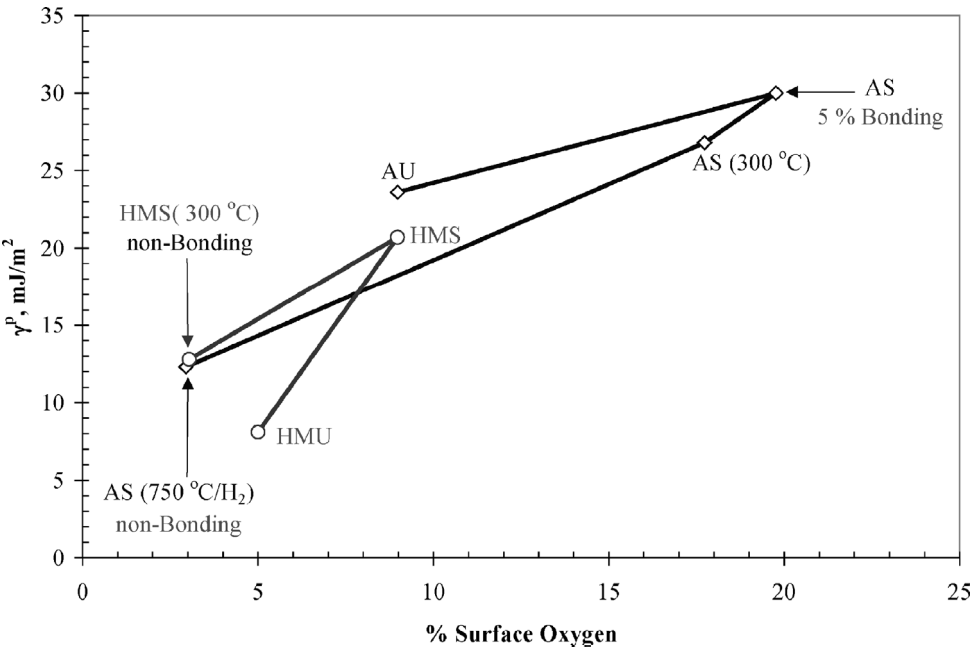
Figure 3. Plot of the polar component of graphite fiber surface free energy (γ^p) versus XPS determined oxygen content (adapted from Ref. [41]).

between the epoxy matrix and the carbon fiber occurs through covalent bonds. The IFSS in treated carbon fiber/epoxy composites tripled and doubled, respectively, relative to the AU and HMU carbon fiber epoxy composites. By subsequently heat treating the AS and HMS fibers at various temperatures under vacuum, Drzal was able to gradually remove oxygen-containing functional groups from the carbon fiber surfaces. Since the AS fibers have more functional group sites, the effect on the IFSS is more pronounced for this carbon fiber. The heat treatment is consistent with the known decarboxylation reaction of carboxylic acid groups using heat [40]. In the final heating step (750°C) for the AS fiber, Drzal used a hydrogen reducing atmosphere to eliminate as many functional groups as possible and render the fiber surface essentially non-bonding. Drzal inferred from these data that 86% of the adhesion in the AS fibers is due to the removal of the weak outer layer, while covalent bonding contributed 14% to the observed adhesion.

The polar component of the surface free energy on the AS fiber surface treated at 750°C (AS (750°C/H$_2$)) is similar in value to the HMS fiber treated at 300°C (see Fig. 3). This polar component provides another measure of the interaction between the fiber and the matrix. One can infer from this observation that the difference in adhesion between carbon fibers AS (750°C/H$_2$) and the HMS (300°C) is mainly due to fiber surface topography or the mechanical interlocking mechanism (see Fig. 2).

1.3. Glass fiber composites

1.3.1. The fiber interphase (FI) region. As noted by Dwight *et al*. [42, 43], reinforcement-quality glass fibers are drawn from high temperature alloy 'bushing' tips ($>1000°$C) at high cooling rates and linear speeds into a water mist, prior to the application of the sizing. This process generates on the top 100 μm of the unsized fibers a fiber interphase (FI) region whose composition and structure are unique from the bulk glass.

Although attempts to quantify the features of the FI region with modern surface analysis instruments have met with only limited success, it is generally accepted that the application of water to the just formed glass fibers destroys the highly strained surface Si—O—Si bonds by a dissociative chemisorption reaction that forms silanol groups (SiOH) on the glass fiber surface. Although good adhesion and composite strength were found in early glass resin composites when the resin (e.g. polyester) was bonded directly to the glass surface, these properties were lost when the composites were exposed to moisture.

1.3.2. The fiber interphase (FI)-sizing interphase (SI) interface and sizing interphase (SI) region. In 1947, R. K. Witt *et al*., in a 'confidential' report to the Navy Bureau of Ordnance, observed that allyltriethoxysilane (bonding silane) on glass fibers gave polyester composites with twice the strength of those treated with ethyltrichlorosilane (non-bonding silane) [18]. In addition, the flexural strength retention under wet conditions of polyester laminates treated by a nonaqueous solvent treatment of vinyltrichlorosilane was greater than the original dry strength of a polyester laminate composed of unsized fibers [44].

Following this lead, Plueddemann *et al*. [45] evaluated over a hundred different organofunctional silanes as coupling agents for use in glass-reinforced polyester and epoxy composites. As a result, glass fibers are often treated with a 'sizing' package composed of organofunctional silanes (silane coupling agents (SCAs)) along with surfactants and functionalized organic molecules. Consistent with Plueddemann's early research results, the 'sizing' package is designed to provide stability to the fiber–matrix interphase in adverse environmental conditions, protect the glass surface during processing and adverse environmental conditions, and promote adhesion between the matrix and glass fiber. The first two functions of the 'sizing' package contrast the behavior of carbon fibers, which are resistant to environmental attack.

Industrially, the 'sizing' packages are deposited from aqueous solution under acidic conditions. Since industrial sizing packages are proprietary and the SCA is primarily responsible for interphase stability, most fundamental research on SI interphases focuses on SCA film morphology on the glass surface. Hence, the SI is really a silane interphase (*SiI*). Using this approach, the research teams of Ishida, Koenig, *et al*. [14, 16, 46, 47] and Johannson *et al*. [48] have shown that the *SiI* film on the glass surface, has a complex multi-layer structure consisting of chemisorbed and physisorbed silanes. The chemisorbed silanes are bonded to the glass fiber

surface and to each other via siloxane bonds. These siloxane bonds are formed as the silanol groups on the glass fiber surface and on the hydrolyzed SCAs condense and eliminate water. Depending on the deposition process, exposure time, the substrate, and the SCA type, chemisorbed silanes may form a film that is several layers thick with varying degrees of siloxane bonding between SCA molecules. Tutas *et al.* [49] reported thicknesses of the *SiI* absorbed on glass surfaces between 50 and 200 μm.

Hydrolytic studies have confirmed the existence in the chemisorbed region of tightly bound and loosely bound layers. The loosely bound layers are characterized as those SCA molecules whose siloxane bonds are hydrolyzable by boiling water. Hence, the siloxane film that remains after hydrolysis by boiling water is classified as tightly bonded to the glass fiber surface. The chemical bonding between these SCA molecules and the FI region on the glass surface form the basis for the FI-SI interface.

By the current deposition processes and hydrolytic studies, it is generally accepted that more than a monolayer of silane is needed to yield the optimum strength of a composite material. This is assumed to result from the need for interfacial chemical bonds, interpenetrating network formation in the chemisorbed silane layers, and proper orientation of the organofunctional groups. For the latter it has been shown by Boerio *et al.* [24] and Ishida, Koenig, *et al.* [13] that γ-aminopropyl triethoxysilanes deposited from aqueous solutions form predominately cyclic ring structures in the *SiI*. The chemisorbed silane layer is believed to be responsible for the reinforcement mechanisms in the fiber–matrix interphase region.

Physisorbed silanes are characterized as those silanes that are readily removed from the surface by washing with an organic solvent that does not cleave siloxane bonds. Ishida, Koenig, *et al.* suggest that these silanes migrate into the matrix interphase (MI) regions and reduce, through plasticization, the fiber–matrix interface strength and flexural strength of the composite. Therefore, this region is undesirable from a mechanical property perspective, even though it has been noted that physisorbed silanes during processing act as a lubricant. From these data, the optimal interphase region consists of a FI-SI interface and a silane interphase region composed of chemisorbed layers.

1.3.3. The SI-matrix interphase (MI) interface and the matrix interphase (MI) region. Adhesion between the fiber and the matrix is effected at the SI-MI interface. Because of the complex multi-layered structure that usually characterizes the silane and sizing interphases (see previous section), the SI-MI interface is not a contiguous and flat structure. In this multi-layered structure, adhesion is achieved through mechanical interlocking, physicochemical interactions and chemical bonding (see equation (1)). As with carbon fibers, the simplest interface for effecting adhesion between the fiber and matrix is formed by the direct interaction of the bulk matrix, typically an epoxy-amine resin, with the bare (or unsized) glass fiber (i.e. FI-MI interface).

Table 1.
Interface properties for bare and epoxy sized E-glass composites [50]

Interface test	Bare E-glass fibers (MPa)	Epoxy sized E-glass fibers (MPa)
Microindentation test	44.6 ± 3.0	60.1 ± 3.3
Short-beam shear test	71.3 ± 1.6	80.2 ± 2.2
90° flexural property test	75.6 ± 1.8	102.0 ± 5.2
0° flexural property test	1010 ± 60	1260 ± 50

Although the environmental instability and adhesion strength of this simple FI-MI interface was known from the research of Bjorksten [44] and Plueddemann *et al.* [18, 45], Drzal [50] compared the interface strength and failure behavior of bare E-glass fiber composites with composites composed of commercial epoxy-compatible sized E-glass fibers (see Table 1). The numbers after the ' $\pm$ ' sign in Table 1 represent one standard deviation about the reported mean values. The E-glass fibers were embedded in a DGEBA epoxy resin cured with the aliphatic diamine-curing agent, 1,2-diaminocyclohexane (DACH). In this system, Drzal found that the interfacial shear strength, as measured by the single-fiber microindentation test, of the bare E-glass fiber composite was significant, but approximately 35% lower than the epoxy sized E-glass fiber composite. In addition, the fiber–matrix interface for the bare E-glass single fiber composite failed by debonding, while the epoxy sized E-glass single fiber composite failed by debonding with matrix crack formation. The matrix cracks resulted in specimen failure and precluded interfacial shear strength testing using the SFFT technique. A fractional difference of 35% was also observed for the 90° flexural properties of the unidirectional composites, where the fiber–matrix interphase is the controlling factor. A smaller difference was observed from the fiber dominated 0° flexural test. The lower strength value for the epoxy sized E-glass composite was attributed to the change in failure mode associated with fiber fracture. During the 0° flexural test, the bare E-glass fiber laminates exhibited controlled failure by propagating delaminations along the tensile surface of the specimen. In contrast, the epoxy-sized E-glass fiber laminates failed catastrophically. Finally, only a fractional difference of 12% in interlaminar shear strength (ILSS) was obtained between the laminates in the short beam shear test. All specimens failed in shear at or near the midplane. Drzal suggested that the coalescence of the matrix cracks into critical sized flaws on the tensile surface might be responsible for the small difference observed.

In structural applications where controlled fiber failure is important, these tests suggest that the bare E-glass fiber composites should be chosen. However, this type of fiber–matrix interphase, as noted above, has been shown, experimentally, to be unstable in moisture rich environments. Theoretically, Kinloch *et al.* [51] calculated that the works of adhesion between epoxy resin and silica, ferric oxide, and aluminum oxide substrates are positive, indicating thermodynamic stability,

when only the surface energies are considered. In the presence of water, the works of adhesion of these systems are negative and indicate instability of the substrate-matrix interphase. Since silicate glasses contain metal cations, Kinloch expects the work of adhesion of silica glasses to be more negative than silica in the presence of absorbed water. This has led Pocius [10] to note: 'if one expects to have an adhesive bond in adverse environmental conditions, provide for interfacial covalent bonding'.

Ahagon and Gent [52] first illustrated the relationship between chemical bonding and the work of adhesion at a *SiI*-MI interface by depositing mixtures of vinyl triethoxysilane (bonding) and ethyl triethoxysilane (non-bonding) on Pyrex glass plates (substrate) to control the level of adhesion between the substrate and anionically polymerized polybutadiene. Since the elastomer is viscoelastic, the work of adhesion was extrapolated to zero strain rate and compared with the concentration of vinyl groups on the surface. An approximately linear dependence was found. In 1996, Hunston *et al.* [53] extended the research of Ahagon and Gent to investigate the affect of chemical bonding on the fiber–matrix interfacial shear strength in composites. Using non-aqueous mixtures of *n*-octadecyl trichlorosilane (non-bonding) and γ-aminopropyl triethoxysilane (bonding), these researchers found that the interfacial shear strength was dependent on the degree of covalent bonding at the *SiI*-MI interface. Although the research of Hunston *et al.* [53] assesses the change in IFSS with covalent bonding, there have been no fundamental studies comparable to the research performed by Drzal on carbon fibers that allow for elucidating the contribution the other adhesion modes have on the overall interfacial shear strength.

The properties of the MI are influenced by the choice of SCA and the SCA deposition process. The existing body of literature on composite interphases indicates that the modulus and toughness of this region strongly influence the early stages of composite failure behavior. For *SiI* interphases composed of chemisorbed and physisorbed silanes, Ishida and Koenig [12] have reported that the MI can vary between 200 Å and 20 000 Å. Recently [54], the MI interphase region formed by the reaction of DGEBA with bis(*p*-aminocyclohexyl)methane (PACM20) on an aluminum surface was determined by using spatially resolved electron energy-loss spectroscopy (EELS) in a scanning transmission electron microscope (STEM) to be approximately 90 Å. The MI was enriched in PACM20 as indicated a gradual compositional change from 25 ± 5 vol% PACM20 in the bulk epoxy to 80 ± 15 vol% PACM20 at the epoxy/oxide interface.

1.4. Schematics of interphase deformation behavior

Drzal [19], Ishida and Koenig [12], and Bascom [32] have researched the response of these regions to fiber fracture and increased deformation. Extending the matrix responses delineated by Bascom to include the research results of Drzal and Ishida and Koenig, the primary responses of the fiber–matrix interphase are given schematically in Fig. 4.
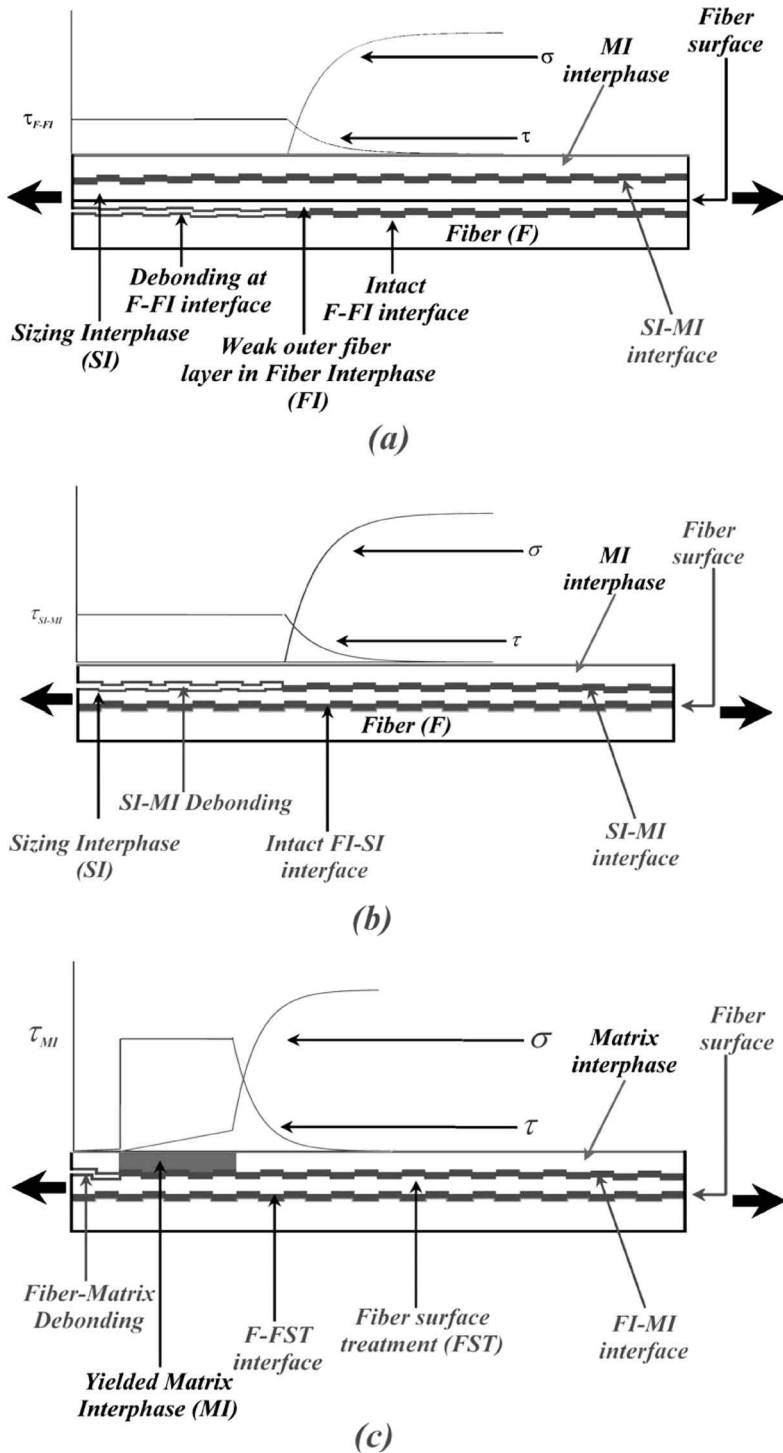
Figure 4. Schematic of interphase deformation behavior (adapted from Refs [32], [12] and [19]).

The mechanical response of the fiber–matrix interphase region to the shear stress at a fiber break site has three primary responses. As the applied load increases (a) the shear strength of the FI is reached ($\tau_{F\text{-}FI}$), (b) the adhesion strength at the SI-MI (shown) or FI-MI interface is exceeded ($\tau_{SI\text{-}MI}$ or $\tau_{FI\text{-}MI}$), or (c) the shear strength of the MI is reached (τ_{MI}). In the first case, the stress-transfer length or ineffective length would increase by debonding of the weak outer fiber layer from the fiber core. Increasing the transfer length has the net effect of reducing the determined value of the interfacial shear strength. This failure mode has been observed in untreated *type A* carbon fibers, which was shown by Drzal [19, 20] to have a mechanically weak outer fiber layer that limited the interfacial shear strength of the fiber–matrix interphase region. This weak interface layer is generally removed during the treatment phase of carbon fiber production.

Since carbon and glass fiber fracture is a brittle failure process, some interphase failure along the length of the fiber (debonding) always occurs during fiber fracture. The extent of this debonding depends on the fiber–matrix interfacial shear strength and the fracture toughness of the matrix interphase (MI) region. For interfaces with low interfacial shear strength, the length of the initial debond region increases with increased deformation (secondary debonding). Since weak frictional forces control stress transfer in the debonded region, the stress transfer length increases in this failure mode. Galiotis *et al.* have observed this mode in carbon fiber epoxy composites [55].

For cases where adhesion in the interface regions is good, yielding of the MI region is the dominant mechanism increasing the stress-transfer length. Research by Carrara and McGarry [56], Holmes *et al.* [57, 58], and Galiotis [59], suggests that the degree of matrix yielding is influenced by stress concentrations in the fiber break region and the viscoelastic behavior of the matrix interphase region. In general, MI yielding increases the stress-transfer length to a lesser degree than the previous two failure modes.

Although these schematics provide a qualitative description of the deformation response of the fiber–matrix interphase, methodologies (especially for glass fiber composites) that admit assessment of the interphase response to deformation when the interphase morphology and chemical interaction mechanisms are systematically controlled have not been generally available. The major problem with glass fiber composites arises from the fact that the morphology and adhesion of the deposited silane-coupling agent cannot be controlled sufficiently to admit systematic adhesion studies.

Although silane coupling-agents deposited by self-assembled monolayer (SAM) technology have no current industrial relevance, recent technology developments [30] in the deposition of functionalized SAM monolayers may provide a key to controlling the morphology and adhesion of the silane-coupling agent (SCA) layer deposited on glass fibers. With this approach, the contribution that the various adhesion mechanisms have on fiber–matrix interface strength can be systematically investigated.
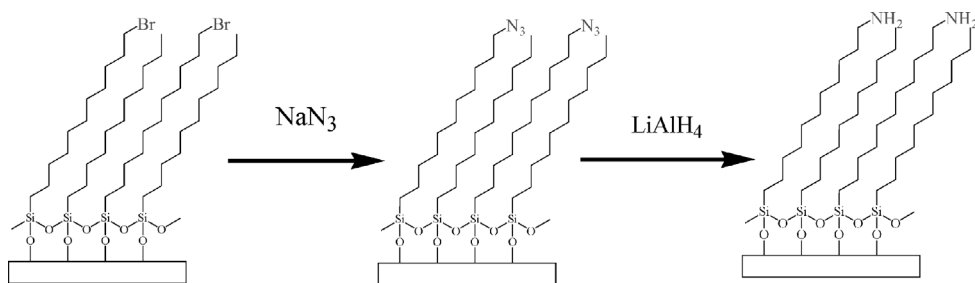
2. RESEARCH APPROACH

For the E-glass fibers investigated in this research, the simplest form of the SI, which includes covalent bonding at the FI-MI interface, involves the deposition of only a monolayer of silane-coupling agent (SCA) onto the E-glass surface. Assuming that the glass fiber has a uniform structure everywhere except on the glass surface, where reactive silanols exist and covalently bond to the SCA, the FI interphase region would include a glass surface (GS)–SCA interface and the SCA interphase region. This simplified FI should minimize the complexity of the MI region. In addition, the deposition of a monolayer of SCA on a smooth glass fiber surface should afford a FI-MI interface where mechanical interlocking is minimized. By controlling the active bonding sites on the fiber surface, the impact of physicochemical interactions and chemical bonding on the fiber surface can be evaluated independently. In addition, comparing the mechanical response of the SAM films to SCA films from deposition processes that form multi-layer SCA films, the impact of mechanical interlocking on fiber–matrix adhesion can be investigated.

Chemical bonding at the FI-MI interface can either be covalent, hydrogen bonding, or ionic in nature. By controlling the type of functional group, the influence of these groups on fiber–matrix adhesion and MI toughness can be investigated. In this research paper we will be particularly interested in how amine and hydroxyl functional groups influence FI-MI interface adhesion.

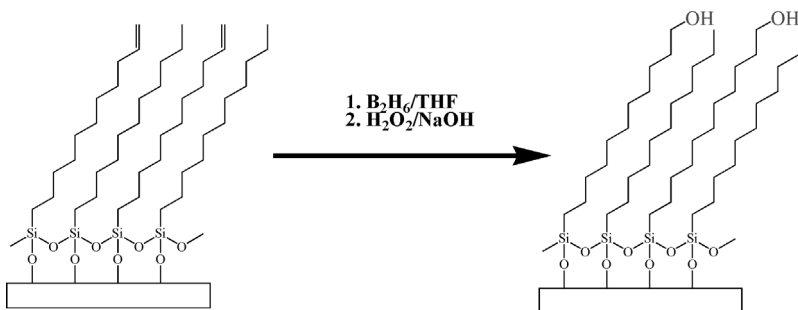### 2.1. Prior research on amine functionalized SAM films

In 1990, Balachander and Sukenik [28] appear to be the first to report the creation of functionalized self-assembled monolayers (SAMs) by using trichlorosilanes that were later converted to the desired functionalility using *in situ* nucleophilic substitution. In 1996 and 1997, the research teams of Fryxell *et al.* [29] and Heise, Menzel, *et al.* [30] reported the preparation of mixed SCA layers deposited on silicon wafers using this methodology. Of particular interest in the Heise *et al.* paper are the procedures describing the conversion of mixed SAMs of bromo- and alkyl-terminated SCAs to mixed SAMs of amino- and alkyl-terminated SCAs. As shown in Fig. 5, the bromine functionality is converted to the amine functionality by the *in situ* reaction with sodium azide followed by reduction with lithium aluminum hydride. For the bromo- and alkyl-terminated SCA used in the research Heise *et al.*, have reported a yield of approximately 80% for the conversion of the bromine by azide. The yield for subsequent reduction to the amine is reported to be approximately 100%.

Using this research as a template, a research program formulated for E-glass fiber composites was designed at NIST to assess the contribution to FI-MI interface adhesion of the first three factors described by Sharpe and Drzal and expressed mathematically by the Nardin and Ward equation (see equation (1)).

Schematic of the *in situ* modification of mixed amine SAMs

Figure 5. Reaction schematic detailing the preparation of mixed amine SAMs (adapted from Ref. [30]).

Schematic of the *in situ* modification of mixed hydroxyl SAMs

Figure 6. Reaction schematic detailing the preparation of mixed hydroxyl SAMs (adapted from Ref. [60]).

2.2. Prior research on hydroxyl functionalized SAM films

Cave and Kinloch [60], using the research of Netzer *et al.* [61, 62] as a reference, functionalized vinylic SAMs via a hydroboration reaction using diborane followed by oxidation using alkaline hydrogen peroxide, to form a terminal hydroxyl group (see Fig. 6). Prior research in the NIST laboratory using the DGEBA/m-PDA epoxy resin system [57] and by Drzal *et al.* [50] using the DGEBA/DACH epoxy resin system has shown that interphase failure in model composites using bare E-glass fibers in these resin systems proceeds primarily by interface debonding. This occurs even though the IFSS is comparable to that found with amine SCAs, which fail by interface debonding with matrix crack formation. For the DGEBA/DACH system, Drzal has shown that this change in behavior at the micromechanics level translates into a change in the macroscopic failure behavior of the composites (i.e. non-catastrophic to catastrophic). Since the bare E-glass fiber surface is composed of silanol groups, this system will be used to gain a better understanding of the role hydroxyl groups play on adhesion between bare E-glass fibers and amine-cured epoxy resins.

3. EXPERIMENTAL

Silane coupling agents used in the FI-MI interface bonding study include (1) γ-aminopropyl trimethoxysilane (γ-APTMS), (2) propyl trimethoxysilane, (PTMS), (3) γ-aminopropyl trichlorosilane (γ-APTCS), (4) propyl trichlorosilane (PTCS), (5) 11-aminoundecyl trichlorosilane (11-AUTCS), (6) undecyl trichlorosilane (UTCS), and (7) 11-hydroxylundecyl trichlorosilane (11-HUTCS). APTMS, PTMS, PTCS, and UTCS are commercially available and were used from the supplier without further purification.

3.1. Synthesis of 11-AUTCS, γ-APTCS and 11-HUTCS

11-AUTCS, γ-APTCS and 11-HUTCS were synthesized in the laboratory using the templates provided in refs [30] and [60] as a guide. 11-Bromoundecyl trichlorosilane (11-BrUTCS) and γ-bromopropyl trichlorosilane (γ-BrPTCS) are the precursor materials for 11-AUTCS and γ-APTCS, respectively. These precursor materials are available commercially. The precursor material for synthesizing 11-HUTCS is 10-undecenyl (vinyl-terminated) trichlorosilane (10-U(en)TCS). This material is not available commercially and was synthesized in the laboratory from commercially available 10-undecenyl alcohol.

Fourier transform infrared (FTIR) spectroscopy and ^{1}H, ^{13}C, and ^{28}Si nuclear magnetic resonance (NMR) spectroscopy were used to characterize the synthesized materials. The details of the synthesis procedure and their characterization results will be published elsewhere.

The vinyl- and bromo-silanes were deposited onto the substrates to achieve SAMs or simulate the SAM deposition process for a comparison between short- and long-chain trichlorosilanes deposition behavior. These silane layers were then activated *in situ* to the desired terminal group by the procedures described below.

3.2. E-glass fiber preparation

A 30 cm long tow was cut from a spool of E-glass fibers (from Owens-Corning) (average fiber diameter of 15 μm) previously shown to be bare with no processing aids by X-ray photoelectron spectroscopy (XPS) [58]. The acetone (spectrophotometric-grade) washed tows were vacuum dried at 110°C for 2 h, and cooled prior to use.

3.3. Adsorption of the silanes onto E-glass fibers

3.3.1. Aqueous adsorption of γ-APTMS and PTMS. A 4.5×10^{-3} mol/l silane mixture, APTMS and PTMS, in water was prepared and the pH adjusted from 3 to 4 with a 2 M HCl solution. A digital pH meter (PHH 320 Omega Engineering Inc) with a standard glass electrode was used to determine the pH value of the coupling agent solution. The ratio of APTMS and PTMS in the mixture was varied to produce intermediate degrees of bonding between the glass fiber and epoxy. The silane solution was stirred for 1 h. The coupling agent solution was then coated on

clean E-glass fibers by dipping the fiber tow in the silane mixture for 2 min. The tow was removed and allowed to air-dry overnight at room temperature, followed by vacuum oven drying for 1 h at $110°C$ and -20 kPa. The coated fibers were cooled prior to use.

3.3.2. Non-aqueous adsorption of long-chain (11-BrUTCS/UTCS and 10-U(en) TCS/UTCS) and short-chain trichlorosilanes (γ-BrPTCS/PTCS). The solution was prepared by mixing the desired ratio of bromo-terminated trichlorosilane and methyl-terminated trichlorosilane (a volume fraction of 0.3% solution in hexadecane) in a 400 ml vial. The acetone-cleaned fibers were immediately immersed in the silane solution. The vial was then placed in an oven, and heated to $40-50°C$ for $4-6$ h. Subsequently the coated substrates were withdrawn from the solution and carefully handled by rinsing with methylene chloride. The substrates were further rinsed with acetone.

Adsorption mixture of vinyl-terminated trichlorosilane (10-U(en)TCS) and methyl terminated trichlorosilane (UTCS) was conducted similar to that described for the bromo-terminated trichlorosilane and methyl-terminated trichlorosilane systems.

3.4. In situ *modifications*

3.4.1. Azide-terminated SAMs. The bromo-terminated mixed SAMs substrates were placed in a supersaturated solution of NaN_3 in dry DMF (1.5 g in 100 ml). The solution (together with the undissolved NaN_3) was stirred at room temperature. After 24 h the substrate was rinsed with distilled water (see Fig. 5).

3.4.2. Amino-terminated SAMs. The azide-terminated SAMs substrates were placed in lithium aluminum hydride solution (0.2 mol/l in THF). After 24 h, the SAMs modified substrates were immersed in THF for an additional 24 h. The modified SAMs substrate were then placed in a volume fraction of 5% HCl solution for 5 h to complete the hydrolysis of the aluminum complex. The modified substrates were then rinsed with distilled water, followed by acetone and then placed in triethylamine for 24 h to convert the terminal $-NH_3^+$ groups into $-NH_2$ groups. The SAMs modified glass surface was then dried for 1 h (see Fig. 5).

3.4.3. Hydroxyl-terminated SAMs. The vinylic-terminated SAMs substrates were dipped for two minutes into a 1 M solution of diborane in THF. This solution was kept under dry argon atmosphere at room temperature. The substrate was then dipped for an additional two minutes in a volume fraction of 30% hydrogen peroxide solution in 0.1 mol/l NaOH and then rinsed using distilled water before drying using hot air (see Fig. 6).

3.5. *Characterization of SAMs coatings*

Dynamic contact angle (DCA) measurements were used to characterize the coated fibers. Parallel depositions were performed on silicon wafers and glass plates

as substrates. These films were characterized using contact angle (DCA and static) measurements, ellipsometry, and tapping mode atomic force microscopy (TMAFM), diffuse reflectance infra-red Fourier transform (DRIFT) spectroscopy, and X-ray photoelectron spectroscopy (XPS), the results of which will be published elsewhere.

3.6. Fragmentation test

3.6.1. Test description. The single fiber fragmentation test (SFFT) is an indirect micromechanics method used to calculate the degree of adhesion between a rigid fiber and a more ductile polymeric matrix in fiber-reinforced polymer composite. In a single fiber fragmentation test, typically, the fiber is embedded in a matrix material with a higher strain-to-failure than the fiber and the fiber breaks when longitudinal strain is applied. The test is performed in the NIST laboratory by the sequential application of strain increments. The breaks occur at flaws along the fiber length, in a progressive way from the most critical flaw to least critical flaw. A saturation limit is eventually attained, when the fragmented fiber is made up of a large number of very short fragments. Upon reaching the saturation limit, any additional strain does not cause further failure of the fiber. The resulting distribution of fiber fragment lengths represents the raw data from the single fiber fragmentation test.

3.6.2. SFFT specimen preparation. The molds for preparing SFFT specimens were made with silicon rubber (General Electric) following the procedure described by Herrera-Franco and Drzal [63]. All molds were post cured at 150°C and rinsed with acetone prior to use. Single filaments of coated E-glass fiber were carefully separated from the 30 cm tow. The individual fibers were aligned in the mold cavity via the sprue slots in the center of each cavity. The cleaned or modified fibers were temporarily fixed in place by pressing them onto double-stick tape. Small strips of double-stick tape were placed over each fiber end to hold them in place until each fiber was permanently mounted with 5-min epoxy (see Fig. 7).
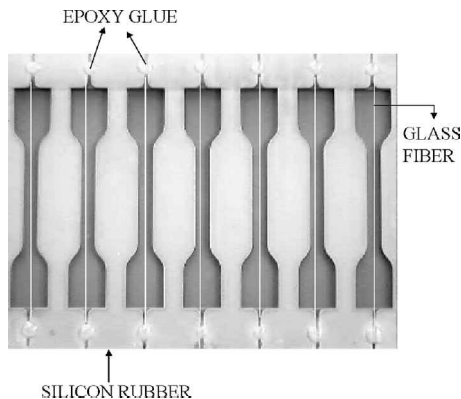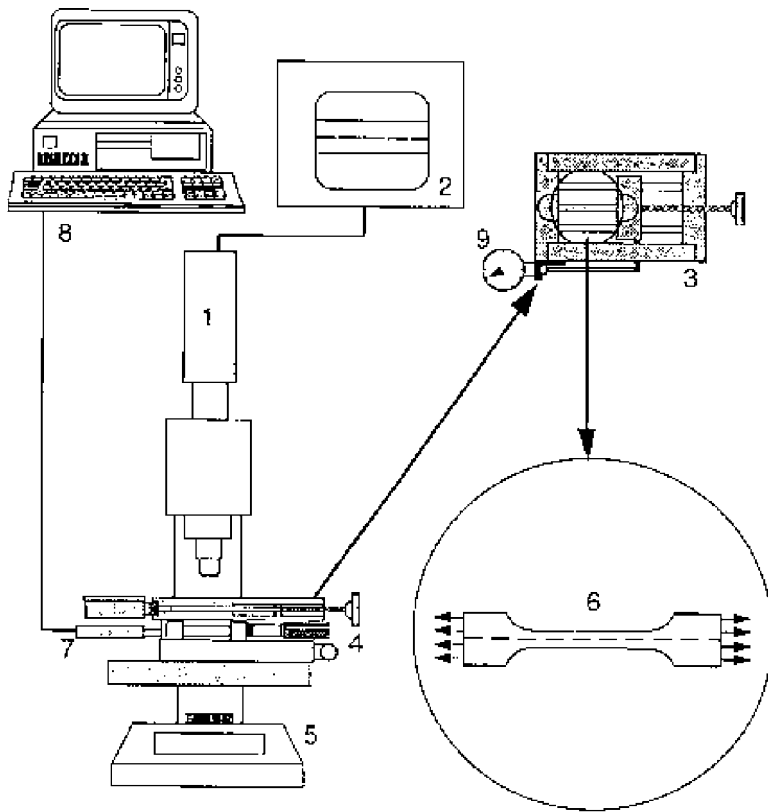

Figure 7. Molds for preparing SFFT specimens.

The SFFT specimens were prepared with an epoxy (diglycidyl ether of bisphenol A, DGEBA, Epon 828, Shell) cured using *meta*-phenylenediamine (m-PDA, Fluka Chemical). One hundred grams of DGEBA and 14.5 g of m-PDA were weighed out in separate beakers. To lower the viscosity of the resin and melt the m-PDA crystals, both beakers were placed in a vacuum oven (Fisher Scientific Isotemp Vacuum Oven, model 281 A) set at 65°C. After the m-PDA crystals were completely melted, the silicone rubber molds containing the fibers were placed into another vacuum oven (Fisher Scientific Isotemp Vacuum Oven, model 281 B) that was preheated to 75°C at −20 kPa, for 20 min. This last procedure dries the mold and minimizes the formation of air bubbles during the curing process. At approximately 9 min before the preheated molds were removed from the oven, the m-PDA is poured into the DGEBA and mixed thoroughly. The mixture was placed into the vacuum oven and degassed for approximately 7 min. After 20 min, the preheated molds were removed from the oven and filled with the DGEBA/m-PDA resin mixture using 10 ml disposable syringes. The filled molds were then placed into a programmable oven (Blue M, General Signal, model MP-256-1, GOP). A cure cycle of 2 h at 75°C followed by 2 h of post curing at 125°C was used.

3.6.3. SFFT apparatus. The fiber fragmentation tests were carried out on a small hand operated loading frame similar to that described by Herrera-Franco and Drzal [63] mounted on a Nikon Optiphot polarizing microscope (see Fig. 8). The image was viewed using a CCD camera (Optronics LX-450 RGB Remote-Head microscope camera) and monitor (Sony, PVM-1344Q). Before the test, the fiber diameter was measured with an optical micrometer (VIA-100 from Boeckeler) attached to the video system. The sample was scanned by translating the loading frame under the microscope with a micrometer. The position of the load frame is monitored by an linear variable differential transformer (LVDT) (Trans-Tek, Inc. model 1002-0012) connected to an A-to-D board (Strawberry Tree, Inc.) in a computer. To measure fragment lengths or other points of interest in the sample, the location was aligned with a cross-hair in the microscope as seen on the video monitor, and the position of the LVDT was digitized into the computer. The standard uncertainty in relocating a point reproducibly is ± 1.1 μm. The load is also monitored during the experiment using a 2224 N (500 pounds) load cell connected to a bridge (load cell and AED 9001A bridge, Cooper Instruments). The expected standard fractional uncertainty of the load measurements is 3% of the load. The bridge is attached to the same computer via a serial connection. A custom program was developed to continuously record changes in the load and displacement.

3.6.4. SFFT testing protocol. Each SFFT specimen was loaded in tension by the sequential application of step-strains. The average application time of each strain step was (1.1 ± 0.2) s and the average deformation was (14.5 ± 3.1) μm, where the

1 TV Camera   5 Microscope
2 TV Monitor   6 Single Fiber Specimen
3 Loading Device   7 Linear Variable Differential Transformer
4 XY Translation Stage   8 Data Acquisition System
                           9 Displacement Gage

Figure 8. Schematic of single fiber fragmentation test machine.

number after the ' $\pm$ ' sign represents one standard deviation about the mean value. The delay time between the applications of successive step-strains was 10 min [58].

3.6.5. Data analysis. The raw data was converted to interfacial shear strength values using the recently developed non-linear viscoelastic (NLVE) shear-lag model [57] and the more common Kelly-Tyson model [64]. The specific methodology for using the NLVE shear-lag model to calculate interfacial shear strength has been published elsewhere [65, 66]. Standard uncertainties reported in this paper were obtained using propagation of error methods [67].

4. RESULTS AND DISCUSSION

4.1. Data on aqueous deposition of γ -APTMS and PTMS

As previously mentioned, industrial 'sizings' coated on glass fibers are generally deposited from aqueous solutions under acidic conditions. Those sizings generally contain surfactants and functionalized organic molecules, generally called film formers. To minimize the complexity of the model interphase, and since most of these sizing packages are proprietary, only the functionalized silane that is primarily responsible for adhesion at the FI-MI interface is used. The average fiber fragment lengths and the IFSSs from the various bonding and non-bonding mixtures of γ-APTMS and PTMS, respectively, are shown in Fig. 9. The error bars represent one standard uncertainty about the reported mean values. The *x*-axis in Fig. 9 and all subsequent figures in this document represent the amount-of-substance fraction of bonding silane groups to the total number of silane groups. As an example, 30% APTMS — a bonding silane — in solution means that for every mole of silane added to the aqueous or non-aqueous carrier medium 0.3 of a mole was APTMS. The remainder consists of a non-bonding silane, which in the case of Fig. 9 is PTMS, a non-bonding silane. Subsequent references in the paper to an interface / interphase with 50% bonding groups are based on the above definition.
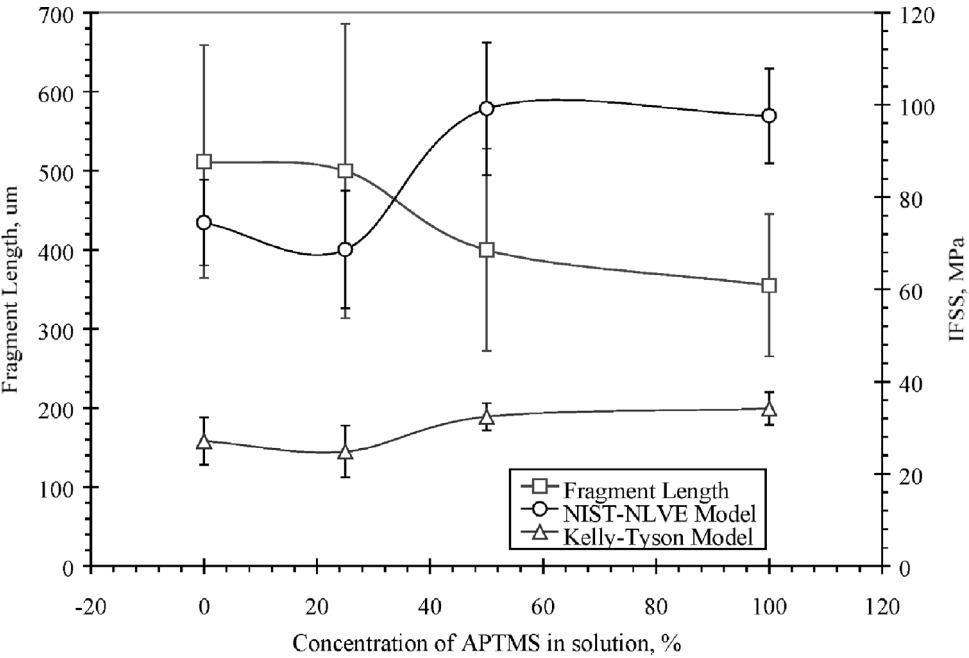

Figure 9. Average fragment length data and calculated IFSS values using the NIST-NLVE and Kelly-Tyson models for mixtures of γ-APTMS (bonding) and PTMS (non-bonding) versus their concentration in the aqueous deposition solution.

The S-shaped curves drawn for each of the data sets are based on single-factor analysis-of-variance (ANOVA) statistics. For the average fragment length, ANOVA statistics suggests that the 0% and 25% bonding group data sets are indistinguishable at the 95% confidence level with a *p*-value of 0.54. However, inter-comparisons for the average fragment lengths of 25% and 50%, and of 50% and 100% bonding groups were indistinguishable with *p*-values of 9.92 E-07 and 4.75 E-04, respectively. The apparent plateau of the fragment length data at the low concentrations may be due to the propensity of the γ-APTMSs deposited from aqueous solutions to form predominately cyclic ring structures in the silane interphase region [13]. This would render the γ-APTMS molecules inaccessible for covalent bonding with the host epoxy resin. Since the 25% bonding SCA layer is predominately hydrophobic in character, the formation of cyclic ring structures at this concentration level may be enhanced.

Consistent with the average fragment data, the S-curve representation is also exhibited in the two IFSS determinations. The *p*-values between 25% and 50% bonding groups that characterized the S-shaped curve break in the NIST-NLVE and Kelly-Tyson models are 0.02 and 0.07, respectively. It should be noted that although the curves in Fig. 9 have been shown to be S shaped, the representation drawn in the figure do not preclude the possibility of other S shaped curves fitting the data.

Arguments by the authors of this paper concerning the validity of the Kelly-Tyson model in the analysis of the DGEBA/m-PDA epoxy resin system have been made previously [57]. In addition, other researchers have found this model to be generally inappropriate for determination of the IFSS of polymeric composites (see references cited in Ref. [57]). However, the analysis is used here in addition to the NLVE model analysis since most researchers are familiar with the Kelly-Tyson data analysis approach.

Interestingly, the average fragment length and both analyses indicate a reasonable amount of adhesion at the FI-MI interface for 0% bonding. A comparison of the average fragment lengths at 0% and 100% bonding shows and increase of only 44% relative to the average fragment length at 100% bonding (i.e. 511 μm and 355 μm, respectively). This translates into an IFSS value of 75 ± 9 MPa or 27 ± 5 MPa for the NLVE and Kelly-Tyson models, respectively. This represents a significant amount of adhesion at the FI-MI interface that, according to Sharpe [11], Drzal [23] and the Nardin and Ward equation [27], must be accounted for by physicochemical interactions and/or mechanical interlocking at the FI-MI interface.

4.2. Data on non-aqueous deposition of 11-AUTCS and UTCS (SAMs)

The average fragment lengths and the IFSSs from the various bonding and non-bonding mixtures for the E-glass fibers treated with 11-AUTCS and UTCS deposited under non-aqueous SAM conditions are shown in Fig. 10. The error bars represent one standard deviation about the reported mean values. Except for the C3 aqueous deposition curve, which was discussed above, all curves through data points in this figure and subsequent figures in this document are illustrative repre-
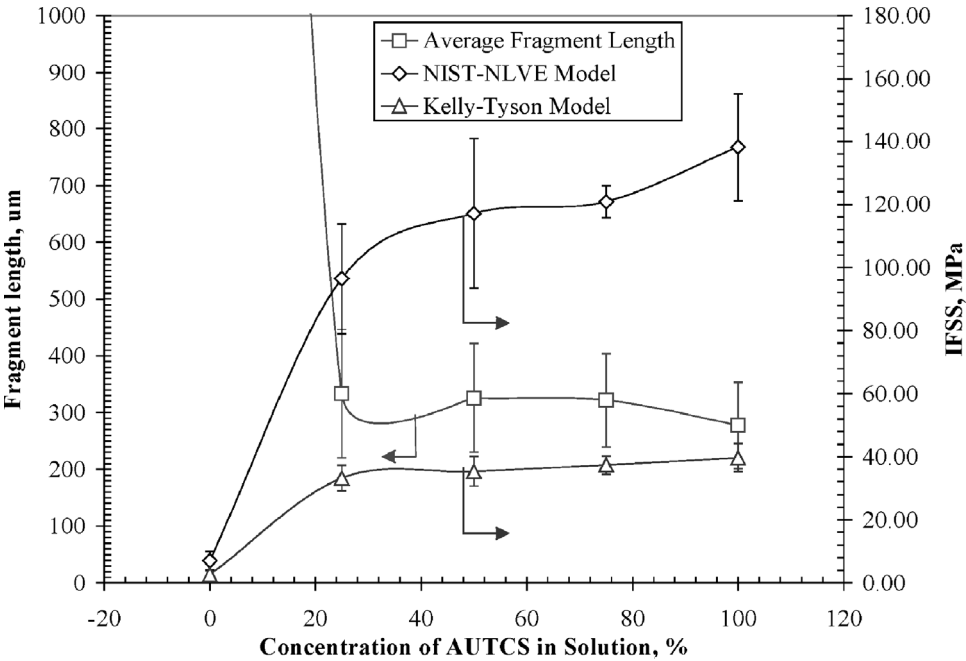
Figure 10. Average fragment length data and calculated IFSS values using the NIST-NLVE and Kelly-Tyson models for mixtures of mixtures of 11-AUTCS (bonding) and UTCS (non-bonding) versus their concentration in the non-aqueous deposition solution.

sentations designed to aid the reader in visualizing each data set. It is immediately obvious from the figure that average fragment length for the E-glass fibers coated with 100% UTCS (0% bonding) is greater than 1000 μm. The actual average value, 4363 ± 1423 μm, is eight times larger than the average fragment length obtained from the non-bonding aqueous specimen, 511 ± 148 μm. As a result, the calculated IFSS using the NIST-LVE or Kelly-Tyson models is extremely low (7 ± 3 MPa and 3 ± 1 MPa, respectively). From the previous section we noted that physicochemical interactions and/or mechanical interlocking must account for the adhesion found in the non-bonding aqueous deposition specimens. Since the deposition of a SAM monolayer should minimize the mechanical interlocking mechanism, we attribute the 7 ± 3 MPa value for the IFSS using the NIST-NLVE model in the non-bonding SAMs interface to physicochemical interactions. Hence, 90% of the 75 ± 9 MPa IFSS value reported for the non-bonding aqueous deposition specimens seems to be due to mechanical interlocking (see Fig. 11).

In Fig. 11, the IFSS for the 100% bonding SAM interface, 138 ± 17 MPa, is larger than the 100% bonding aqueous deposited interface (98 ± 10 MPa). Since the aqueous interface at 0% bonding exhibits adhesion primarily due to mechanical interlocking, the adhesion in the 100% bonding aqueous deposition interface is probably due to a combination of mechanical interlocking and chemical bonding.
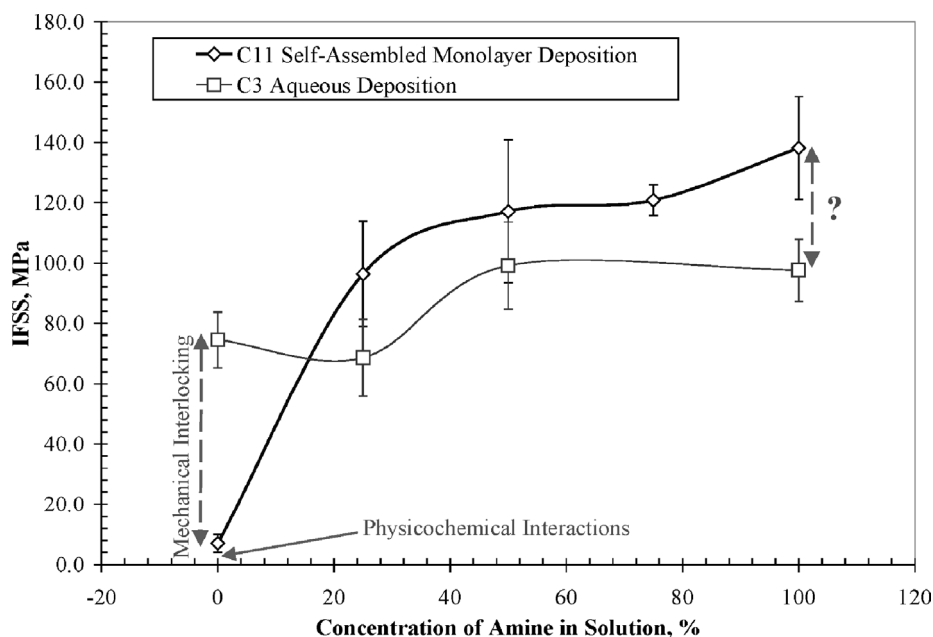
Figure 11. Comparison of IFSS from aqueous deposition of γ-APTMS/PTMS and SAM deposition of 11-AUTCS/UTCS. IFSS data obtained using NIST-NLVE model.

Since the SAM deposition process should minimize the contribution to mechanical interlocking to adhesion in the 100% bonding interface, the IFSS should be due primarily to chemical bonding at the FI-MI interface. The difference in adhesion between the 100% bonding aqueous interface and the 100% bonding SAM interface may be related to the propensity of the γ-APTMSs deposited from aqueous solutions to form cyclic ring structures in the silane interphase region [13]. As we have mentioned before, this would render the γ-APTMS molecules inaccessible for covalent bonding with the host epoxy resin and may limit the maximum attainable IFSS.

4.3. Data on non-aqueous deposition of γ-APTMS and PTMS

To check for evidence that the cyclic ring structure formed by γ-APTMS during the aqueous deposition process may be limiting the maximum attainable IFSS, bonding and non-bonding mixtures of γ-BrPTCS and PTCS were deposited from the non-aqueous solutions generate SAM layers for the mixtures of 11-BrUTCS and UTCS. These silane films were then converted *in-situ* to the amine functional group. It is known that alkyl-chains shorter than C8 do self-assemble; however, the intent of this deposition was to see if the formation of cyclic ring structures could be suppressed and thereby increasing the adhesion at the FI-MI interface. The IFSS data as determined by the NIST-NLVE model is plotted in Fig. 12 along with the
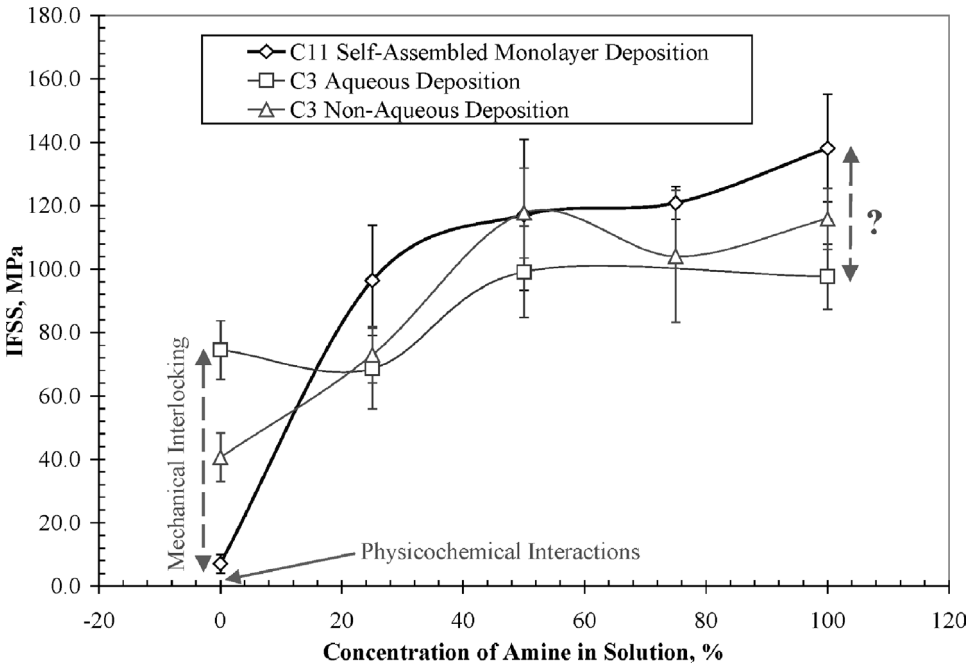
Figure 12. IFSS comparsion from aqueous and non-aqueous depositions of γ-APTMS/PTMS and SAM deposition of 11-AUTCS/UTCS. IFSS data obtained using NIST-NLVE model.

data given in Fig. 11. The error bars represent one standard deviation about the mean.

From these data, the interfacial shear strength with 100% bonding groups on the surface is higher for the non-aqueous deposition, but lower than the SAM deposition process using 11-AUTCS. This is consistent with the assumption that the concentration of cyclic ring structures would be minimized in the non-aqueous deposition process. At 0% bonding the IFSS of the non-aqueous γ-APTMS/PTMS is also intermediate between the aqueous and SAM deposition processes. This may be due to the formation of a more ordered or less porous silane interphase forming on the surface and hence minimizing penetration by the host matrix into the silane interphase. This would have the effect of reducing the contribution to adhesion by the mechanical interlocking mechanism.

4.4. Data on non-aqueous deposition of 11-HUTCS and UTCS (SAMs)

In the introduction section it was noted that Drzal using a DGEBA-DACH epoxy resin compared bare E-glass fiber composites with epoxy-sized E-glass fiber composites and found by the microindentation test that the IFSS for the bare E-glass fiber composites was lower than the epoxy-sized E-glass fiber by about 35%. Previous research from the NIST laboratory on bare E-glass fiber embedded in a DGEBA/m-PDA matrix gives the IFSS as approximately 65 MPa, when the test-

ing procedure in the current research is used. This value is also approximately 35% lower than the value obtained for the 100% γ-APTMS interface obtained by aqueous deposition. Drzal also observed in his system that full composite test specimens of the epoxy-sized fiber failed catastrophically whereas the bare E-glass fiber composite failed in a controlled manner. He associated this difference with the propensity of the epoxy-sized fibers to form matrix cracks during fiber fracture.

In the systems researched in this paper, FI-MI interface failure in all model composites whose silane interphase was obtained from solutions containing bonding groups greater than 25% failed by debonding with matrix crack formation during fiber fracture. In some cases these cracks were large enough to cause specimen failure. In contrast, the DGEBA-DACH epoxy resin used by Drzal was too brittle to test the epoxy-size specimens by the SFFT method. However, because of the lack of matrix crack formation the bare-E glass fiber specimens could be taken to a reasonably high strain before failure. These data suggest an interaction between the curing epoxy-amine resin and the glass fiber surface that promotes the formation of a tough MI interphase region. It is known that hydroxyl groups are catalytic on epoxy-amine reactions and react too slowly with epoxy to interfere with this reaction. Hence, in the absence of any further reaction between the surface silanol groups and the epoxy resin, the adhesion at the FI-MI interface should be primarily hydrogen bonding. Therefore, it is worthwhile using the SAM technology to probe the effect of hydroxyl groups on FI-MI interface adhesion and MI formation. A plot of the IFSS data for SAM interfaces formed from mixtures of 11-HUTCS and UTCS is shown in Fig. 13.

From this figure, the maximum IFSS shear strength (approximately 40 MPa) was obtained with 100% of the hydroxyl bonding groups covering the surface. The IFSS value for this system is about 40% lower than the IFSS value obtained from bare E-glass fibers.

The mechanical interlocking mechanism at the FI-MI interface is effectively eliminated with SAM deposition. In addition, hydroxyl–hydroxyl hydrogen bonding is stronger than physicochemical interactions. From the Nardin and Ward equation, which mathematically expresses the Sharpe and Drzal assumptions on interphase adhesion, it can be inferred that in bare E-glass epoxy-amine composites covalent bonds exists between the epoxy resin matrix and the surface silanols.

In 2001, Ochi and Takahashi published a paper [68] looking specifically at the interaction of epoxy-amine resins systems with silica. These authors concluded from their studies that Si—O—C covalent bonds are formed by condensation of the hydroxyl groups of the cured DGEBA-amine epoxy resin and the silanols on the glass surface. The basic amine-curing agent reportedly catalyzes this condensation reaction. Since it is known that the S—O—C groups in alkoxysilanes are readily hydrolyzed by water to silanols and the corresponding alcohol, the covalent bond formed between the silanol groups on the bare E-glass fibers and the hydroxyl groups on the epoxy resin will be unstable in aqueous environments. Therefore, the proposed reaction mechanism by Ochi and Takahashi provides
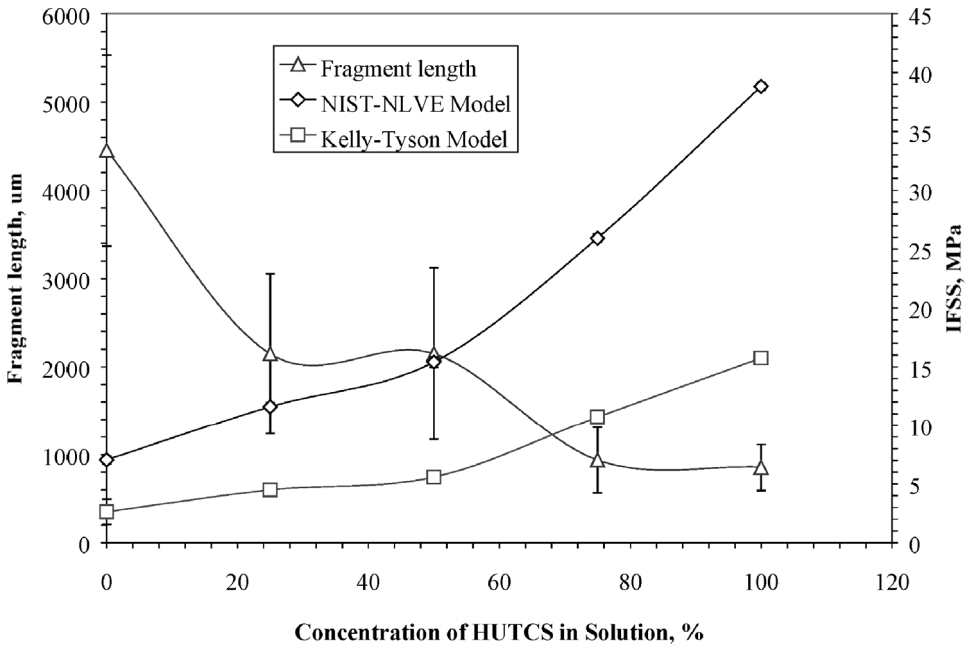
Figure 13. Average fragment length data and calculated IFSS values using the NIST-NLVE and Kelly-Tyson models for mixtures of mixtures of 11-HUTCS (bonding) and UTCS (non-bonding) versus their concentration in the non-aqueous deposition solution.

an explanation for the increased IFSS in the bare E-glass DGEBA-amine epoxy resin systems when the FI-MI interface is not exposed to moisture. In addition, this reaction mechanism also provides, as a companion to Kinloch's theoretical prediction [51], a chemical explanation for the hydrolytic instability of the FI-MI interface formed in composites composed bare E-glass fibers embedded in an epoxy-amine resin.

5. CONCLUSIONS

SAM technology was used to prepare functionalized silane monolayers on E-glass fiber surfaces. Comparing the data from the amine SAM monolayers to silane coupling deposited by aqueous deposition were made and the data were interpreted in terms of the Nardin and Ward equation and the inferences found in Drzal's research which assume the various contributions to adhesion at the FI-MI interface are additive. From this equation, 90% of the IFSS exhibited by the 100% PTMS (non-bonding; IFSS $= 75 \pm 9$ MPa) silane deposited on E-glass fibers under aqueous conditions is due to mechanical interlocking, with the remainder due to physicochemical interactions. For the 100% γ-APTMS (bonding; IFSS $= 98 \pm 10$ MPa) silane deposited on E-glass fibers under aqueous conditions, the IFSS increased by an additional 31% relative to the non-bonding aqueous interface.

Data from the 100% 11-AUTCS SAM (bonding; IFSS $= 138 \pm 17$ MPa) revealed that the strength of this interface exceeded the maximum interfacial shear strength exhibited by the 100% γ-ATMS interface by approximately 40%. This difference was attributed to the formation of the cyclic ring structures shown by Ishida and coworkers [13] to occur when γ-APTMS is deposited from water. Consistent with this interpretation, the IFSS for a 100% γ-aminopropyl silane interface deposited using the non-aqueous SAM approach increased to 116 ± 10 MPa.

The SAMs data also indicate that 70–85% of the maximum IFSS is obtained with 25–50% of the surface covered with functional groups. Kent *et al.* [69] have observed a similar data trend. For the research data published here, two factors may explain this behavior. Steric hindrance, due to the size of the DGEBA molecules, could restrict access to the functional groups on the surface. Therefore, only 35% of the surface functional groups are accessible for bonding. Preferential adsorption of the bromo-terminated C_{11} alkyl SCA relative to the C_{11} alkyl terminated SCA was reported by Heise *et al.* [30]. For the mixed SCA monolayers, this would increase the concentration of the amine functional groups on the surface relative to their concentration in solution. Preferential absorption, however, was not observed by Fryxell *et al.* [29] for mixed SCA monolayers consisting of bromo-terminated C_{17} alkyl and C_{16} alkyl SCAs. Further research will be required to determine the dynamics of the mixed SCA monolayers and their impact on fiber–matrix adhesion.

Hydroxyl SAM interfaces were used to probe the strength of hydroxyl–hydroxyl hydrogen bonding at the fiber matrix interphase. These results were found to be much lower than the adhesion exhibited by bare E-glass fibers embedded in DGEBA/m-PDA epoxy resin. This suggested from the Nardin and Ward model that adhesion between the bare E-glass fibers and the DGEBA/m-PDA epoxy resin involves the formation of covalent bonds. Recently published research by Ochi and Takahashi [68] indicate that the covalent bond formed arises of the amine-catalyzed condensation of the surface hydroxyls and the hydroxyl groups of the amine cured epoxy resin.

REFERENCES

1. *Interfaces in Composites*, ASTM STP 452. American Society for Testing and Materials (ASTM), Philadelphia, PA (1969).
2. H. Ishida and J. L. Koenig, *Composite Interfaces*. Elsevier Science, New York (1986).
3. H. Ishida, *Controlled Interphases in Composite Materials*. Elsevier Science, New York (1990).
4. C. G. Pantano and E. J. H. Chen, *Interfaces in Composites*, Vol. 170. Materials Research Society, Pittsburg, Pennsylvania (1990).
5. L. H. Sharpe, in: *Proceedings of the Sixteenth Annual Meeting of the Adhesion Society, Inc.* Gordon and Breach Publishers, UK (1993).
6. *Composite Interfaces* (1993) (to present).
7. *Journal of Colloid and Interface Science* (1996) (to present).
8. S. M. Lee, *Composite Materials*, Vol. 2. VCH Publishers, New York (1990).

9. R. Yosomiya, K. Morimoto, A. Nakajima, Y. Ikada and T. Suzuki, *Adhesion and Bonding in Composites.* Marcel Dekker, New York (1990).

10. A. V. Pocius, *Adhesion and Adhesives Technology (An Introduction).* Carl Hanser Verlag, Munich (1997).

11. L. H. Sharpe, *Journal of Ahesion* **4**, 51 (1972).

12. H. Ishida and J. L. Koenig, *Polymer Engineering and Science* **18**, 128 (1978).

13. C. H. Chiang, H. Ishida and J. L. Koenig, *Journal of Colloid and Interface Science* **74**, 396 (1980).

14. H. Ishida, in: *Molecular Characterization of Composite Interfaces*, H. Ishida and G. Kumar (Eds), p. 25. Plenum Press, New York (1983).

15. R. T. Graf, J. L. Koenig and H. Ishida, *Journal of Ahesion* **16**, 97 (1983).

16. N. Suzuki and H. Ishida, *Macromolecular Symposia* **108**, 19 (1996).

17. E. P. Plueddemann and G. L. Stark, *Modern Plastics* **51**, 74 (1974).

18. E. P. Plueddemann, *Silane Coupling Agents.* Plenum Press, New York (1991).

19. L. T. Drzal, M. J. Rich and P. F. LLoyd, *Journal of Adhesion* **16**, 1 (1983).

20. L. T. Drzal, M. J. Rich, M. F. Koenig and P. F. LLoyd, *Journal of Adhesion* **16**, 133 (1983).

21. L. T. Drzal, in: *Materials Research Society Symposium Proceedings: Interfaces in Composites*, C. G. Patano and E. J. H. Chen (Eds), p. 275. Materials Research Society, Pittsburgh, Pennsylvania (1989).

22. L. T. Drzal, in: *Proceedings of the Third International Conference on Composite Interfaces (ICCI-III): Controlled Interphases in Composite Materials*, I. Ishida (Ed.), p. 309. Elsevier, New York (1990).

23. J. D. Delong, K. J. Hook, M. J. Rich, J. Kalantar and L. T. Drzal, in: *Proceedings of the Third International Conference on Composite Interfaces (ICCI-III): Controlled Interphases in Composite Materials*, H. Ishida (Ed.), p. 87. Elsevier, New York (1990).

24. F. J. Boerio, L. Armogan and S. Y. Cheng, *Jounral of Colloid and Interface Science* **73**, 416 (1980).

25. F. J. Boerio, L. H. Schoenlein and J. E. Greivenkamp, *Journal of Applied Polymer Science* **22**, 203 (1978).

26. F. J. Boerio and R. G. Dillingham, in: *Adhesive Joints: Formation, Characteristics, and Testing*, K. L. Mittal (Ed.), p. 541. Plenum Press, New York (1982).

27. M. Nardin and I. M. Ward, *Materials Science and Technology* **3**, 814 (1987).

28. N. Balachander and C. N. Sukenik, *Langmuir* **6**, 1621 (1990).

29. G. E. Fryxell, P. C. Rieke, L. L. Wood, M. H. Engelhard, R. E. Williford, G. L. Graff, A. A. Campbell, R. J. Wiacek, L. Lee and A. Halverson, *Langmuir* **12**, 5064 (1996).

30. A. Heise, H. Menzel, H. Yim, M. D. Foster, R. H. Wieringa, A. J. Schouten, V. Erb and M. Stamm, *Langmuir* **13**, 723 (1997).

31. J. A. Manson and L. H. Sperling, in: *Polymer Blends and Composites*, p. 430. Plenum Press, New York (1976).

32. W. D. Bascom, in: *International Encyclopedia of Composites: Composite Materials*, S. M. Lee (Ed.), p. 411. VCH Publishers, New York (1990).

33. G. R. Palmese and R. L. McCullough, *Journal of Adhesion* **44**, 29 (1994).

34. L. T. Drzal, in: *Epoxy Resins and Composites II*, K. Dusek (Ed.), Chapter 1, p. 1. Springer-Verlag, New York (1986).

35. P. Ehrburger, J. J. Herque and J. B. Donnet, in: *5th London International Conference on Carbon and Graphite*, p. 398 (1978).

36. D. M. Brewis, J. Comyn, J. R. Fowler, D. Briggs and V. A. Gibson, *Fibre Science & Technology* **12**, 41 (1979).

37. L. Shechter and J. Wynstra, *Industrial and Engineering Chemistry* **48**, 86 (1956).

38. L. Shechter, J. Wynstra and R. P. Kurkjy, *Industrial and Engineering Chemistry* **48**, 94 (1956).

39. M. R. Alexander and F. R. Jones, *Carbon* **33**, 569 (1995).
40. J. March, *Advanced Organic Chemistry: Reactions, Mechanisms, and Structure*. John Wiley & Sons, New York (1992).
41. G. E. Hammer and L. T. Drzal, *Applied Surface Science* **4**, 340 (1980).
42. D. W. Dwight, T. N. Huff, H. F. Wu, T. A. Malone and A. P. Diwanji, in: *Proceedings of the 27th AVK Conference*, p. 1793 (1996).
43. H. F. Wu, D. W. Dwight and N. T. Huff, *Composites Science and Technology* **57**, 975 (1997).
44. J. Bjorksten and L. L. Yaeger, *Modern Plastics* **29**, 124 (1952).
45. E. P. Plueddemann, H. A. Clark, L. E. Nelson and K. R. Hoffman, *Modern Plastics* **39**, 135 (1962).
46. J. L. Koenig and C. H. Chiang, in: *The Role of the Polymeric Matrix in the Processing and Structural Properties of Composite materials*, J. C. Seferis and L. Nicolais (Eds), p. 503. Plenum Press, New York (1983).
47. H. Ishida, in: *The Interfacial Interactions in Polymeric Composites*, G. Akovali (Ed.), p. 169. Kluwer Academic Publishers, Netherlands (1993).
48. O. K. Johannson, F. O. Stark, G. E. Vogel and R. M. Fleischmann, *J. Comp. Mater.* **1**, 278 (1967).
49. D. J. Tutas, R. Stromberg and E. Passaglia, *SPE Transactions* **4**, 256 (1964).
50. E. K. Drown, H. Al Moussawi and L. T. Drzal, *Journal of Adhesion Science and Technology* **5**, 865 (1991).
51. A. J. Kinloch, W. A. Dukes and R. A. Gledhill, in: *Adhesion Science and Technology*, L. H. Lee (Ed.), p. 597. Plenum Press, New York (1975).
52. A. Ahagon and A. N. Gent, *Journal of Polymer Science: Polymer Physics Edition* **13**, 1285 (1975).
53. D. L. Hunston, K. Macturk, C. Schultheisz, G. A. Holmes, W. G. McDonough and C. L. Schutte, in: *Proc. European Adhesion Conf.*, p. 427. Inst. of Mater., Cambridge, England (1996).
54. D. Arayasantiparb, S. McKnight and M. Libera, *Journal of Adhesion Science and Technology* **15**, 1463 (2001).
55. N. Melanitis, C. Galiotis, P. L. Tetlow and C. K. L. Davies, *J. Comp. Mater.* **26**, 574 (1992).
56. A. S. Carrara and F. J. McGarry, *J. Comp. Mater.* **2**, 222 (1968).
57. G. A. Holmes, R. C. Peterson, D. L. Hunston, W. G. McDonough and C. L. Schutte, in: *Time Dependent and Nonlinear Effects in Polymers and Composites*, R. A. Schapery (Ed.), p. 98. ASTM (2000).
58. G. A. Holmes, R. C. Peterson, D. L. Hunston and W. G. McDonough, *Polymer Composites* **21**, 450 (2000).
59. C. Galiotis, *Compos. Sci. Technol.* **42**, 125 (1991).
60. N. G. Cave and A. J. Kinloch, *Polymer* **33**, 1162 (1992).
61. L. Netzer, R. Iscovici and J. Sagiv, *Thin Solid Films* **99**, 235 (1983).
62. L. Netzer, R. Iscovici and J. Sagiv, *Thin Solid Films* **100**, 67 (1983).
63. P. J. Herrera-Franco and L. T. Drzal, *Composites* **23**, 2 (1992).
64. A. Kelly and W. R. Tyson, *J. Mech. Phys. Solids* **13**, 329 (1965).
65. G. A. Holmes, D. L. Hunston, W. G. McDonough and R. C. Peterson, in: *SAMPE-ACCE-DOE-SPE Midwest Advanced Materials and Processing Conferences*, M. Rokosz, R. B. Boeman, D. T. Buckley and J. Jaranson (Eds), p. 321. Society for the Advancement of Material and Process Engineering (SAMPE), Covina, CA (2000).
66. G. A. Holmes, D. L. Hunston, W. G. McDonough and R. C. Peterson, in: *Proceedings of the 45th International SAMPE Symposium and Exhibition — Science of the Advance Materials and Process Engineering Series*, p. 1114. Society for the Advancement of Material and Process Engineering (SAMPE), Covina, CA (2000).
67. H. H. Ku, *J. Res. Natl. Bur. Stand. — C Engr. and Instr.* **70C**, 332 (1966).

68. M. Ochi and R. Takahashi, *Journal of Polymer Science, Part B — Polymer Physics* **39**, 1071 (2001).

69. M. S. Kent, H. Yim, A. Matheson, J. Sorenson, E. D. Reedy, K. Scjibert and M. Mitchell, in: *Proceedings of the 24th Annual Meeting of the Adhesion Society: Adhesion Science for the 21st Century*, J. A. Emerson (Ed.), p. 300. The Adhesion Society, Blacksburg, VA (2001).